

Magnetic domain structure in nanocrystalline Ni-Zn-Co spinel ferrite thin films using off-axis electron holography

D. Zhang, N. M. Ray, W. T. Petuskey, D. J. Smith, and M. R. McCartney

Citation: *Journal of Applied Physics* **116**, 083901 (2014); doi: 10.1063/1.4891723

View online: <http://dx.doi.org/10.1063/1.4891723>

View Table of Contents: <http://scitation.aip.org/content/aip/journal/jap/116/8?ver=pdfcov>

Published by the [AIP Publishing](#)

Articles you may be interested in

[Nanocrystalline Ni-Al ferrites for high frequency applications](#)

AIP Conf. Proc. **1512**, 408 (2013); 10.1063/1.4791084

[Micro- and nanostructure characterization and imaging of TWIP and unalloyed steels](#)

AIP Conf. Proc. **1430**, 1381 (2012); 10.1063/1.4716378

[Enhanced magnetic properties of Dy³⁺ substituted Ni-Cu-Zn ferrite nanoparticles](#)

Appl. Phys. Lett. **100**, 042407 (2012); 10.1063/1.3679688

[Spin-sprayed Ni-Zn-Co ferrite films with high \$\mu' > 100\$ in extremely wide frequency range 100 MHz–1 GHz](#)

J. Appl. Phys. **93**, 7133 (2003); 10.1063/1.1558198



[Ni-Zn ferrite films with high permeability \(\$\mu' \approx 30\$, \$\mu'' \approx 30\$ \) at 1 GHz prepared at 90°C](#)

J. Appl. Phys. **91**, 7376 (2002); 10.1063/1.1453930



AIP | Journal of Applied Physics

Meet The New Deputy Editors

	Christian Brosseau		Laurie McNeil		Simon Phillpot
---	---------------------------	---	----------------------	---	-----------------------

Magnetic domain structure in nanocrystalline Ni-Zn-Co spinel ferrite thin films using off-axis electron holography

D. Zhang,^{1,a)} N. M. Ray,² W. T. Petuskey,² D. J. Smith,³ and M. R. McCartney³

¹*School of Engineering for Matter, Transport and Energy, Arizona State University, Tempe, Arizona 85287-6106, USA*

²*Department of Chemistry and Biochemistry, Arizona State University, Tempe, Arizona 85287-1604, USA*

³*Department of Physics, Arizona State University, Tempe, Arizona 85287-1504, USA*

(Received 10 June 2014; accepted 18 July 2014; published online 22 August 2014)

We report a study of the magnetic domain structure of nanocrystalline thin films of nickel-zinc ferrite. The ferrite films were synthesized using aqueous spin-spray coating at low temperature ($\sim 90^\circ\text{C}$) and showed high complex permeability in the GHz range. Electron microscopy and microanalysis revealed that the films consisted of columnar grains with uniform chemical composition. Off-axis electron holography combined with magnetic force microscopy indicated a multi-grain domain structure with in-plane magnetization. The correlation between the magnetic domain morphology and crystal structure is briefly discussed. © 2014 AIP Publishing LLC.
[\[http://dx.doi.org/10.1063/1.4891723\]](http://dx.doi.org/10.1063/1.4891723)

I. INTRODUCTION

Soft ferrite materials, such as those based on nickel-zinc-ferrite compositions, are of interest because of their relatively low loss characteristics at high frequencies.¹ Due to technological needs, their applications are being pushed to even higher frequencies into regimes where magnetic properties exhibit limitations. This behavior is often marked by what is referred to as Snoek's Limiting Law, which inversely correlates low frequency permeability, μ' , and resonance frequency, f , as a product, i.e., $(\mu' - 1) \times f$, which is usually constant for a given material structure class and composition.^{1,2} This constancy is generally independent of microstructure and other processing related characteristics, where permeability might decrease because of porosity and cracking, and the resonance frequency correspondingly increases.

These observations tend to hold for ferrite materials with polycrystalline structures comprising of grains that are relatively large in size, on the order of near-sub-micron scales or larger. Increases in the Snoek's product are found in materials where the grain sizes are substantially in the nanometer and mesoscopic scales (i.e., 10–100 nm).^{2,3} Matsushita, Abe, and others have reported such combination of properties in a series of papers on extremely fine grained films of nickel-zinc-ferrite materials which are produced using an aqueous spray deposition technique that they pioneered.³ For instance, the Snoek's product for one of their $\text{Ni}_{0.28}\text{Zn}_{0.18}\text{Fe}_{2.54}\text{O}_4$ films is calculated to be about 26.6 GHz, whereas it is about 1–3 GHz for a bulk ferrite of similar composition.⁴

A detailed explanation of the behavior of nickel-zinc ferrites must correlate comparative structures of the magnetic domains relative to the physical grain structure. In large-grained materials, well-defined, multiple magnetic domains are observed within individual physical grains.^{1,5}

Magnetic domain boundaries interior to nanometer-scaled grains are likely to be too energetic to be prevalent, so that either single magnetic domains are defined concurrently with the physical grains or the magnetic domains must be spread out over multiple physical grains.^{1,5}

The purpose of this paper is to report on a comparison of the magnetic domain structure to the physical grain structure of nickel-zinc-cobalt ferrite films, as imaged by transmission electron microscopy and off-axis electron holography, and atomic force microscopy. The original motivations for this study were to discover whether multi-grained magnetic domains could be directly observed in these materials, and whether the magnetic domains were confined to the physical grain structure.

II. EXPERIMENTAL DETAILS

The ferrite thin films in this work were deposited using a method similar to that developed by Abe and Tamaura.^{6,7} Different materials were used as substrates, which were heated to 90°C during the spin-spray process. In this work, we studied samples with composition of approximately $\text{Ni}_{0.20}\text{Zn}_{0.60}\text{Co}_{0.05}\text{Fe}_{2.15}\text{O}_4$ that were deposited on silicon and glass substrates. Details of the processing conditions are reported elsewhere.² Some of the ferrite films were also deposited directly onto TEM grids with carbon support films: however, only clusters were observed after deposition, indicating that a smooth surface was essential for successful use of the spin-spray coating process. The real μ' and imaginary μ'' permeabilities were measured as a function of frequency using a vector network analyzer with a customized microstrip permeameter.⁸

For cross-section TEM and off-axis electron holography characterization, samples were prepared using cutting, mechanical polishing, followed by dimpling to create thin areas with total thicknesses of about $10\ \mu\text{m}$. Final thinning was done by low energy ($\sim 3\ \text{keV}$) argon-ion-milling giving thin electron-transparent areas of about 200 nm in thickness.

^{a)}Author to whom correspondence should be addressed. Electronic mail: dzhang28@asu.edu

Samples in the plan-view geometry were also prepared, with dimpling and ion-milling done only from the back side of the wafer. A JEOL JEM-4000EX operated at 400 keV with interpretable resolution of 1.7 Å was used for conventional diffraction-contrast and high-resolution phase-contrast imaging, a JEOL JEM-2010F operated at 200 keV was used for annular-dark-field (ADF) imaging and elemental analysis using energy-dispersive X-ray spectroscopy (EDXS), and an FEI CM-200 operated at 200 keV was used for off-axis electron holography observations. This last instrument is equipped with a field emission electron gun that provides a highly coherent electron source and it has a Lorentz minilens located beneath the normal objective lens so that samples can be studied in field-free conditions. Magnetic force microscopy, MFM, measurements were done on the sample surfaces. The equipment used was a home-built atomic force microscope (AFM) which has a cobalt needle probe with a magnetic fringing field that is parallel to the long axis of the needle. This magnetic field interacts with the magnetic field perpendicular to the sample surface and reveals the out-of-plane magnetic domain structure.

III. RESULTS AND DISCUSSION

A. Sample permeability

Figure 1 shows the real and imaginary parts of the complex permeability spectrum of a typical spin-coating film prepared in this study. The purpose of measuring the complex permeability is for use in the comparison of Snoek's Limiting Law. This law states that there is a theoretical limit to the ferromagnetic resonance frequency; however, this value can be exceeded using non-traditional processing techniques.^{1,2,4,9–12} The materials characterized in this study exceeded the theoretical resonance frequency value for conventional nickel-zinc ferrite.^{1,2,4} The Snoek's product for our deposited film is calculated to be 20.1 GHz, which is on the same order of magnitude as the films deposited by Abe *et al.*

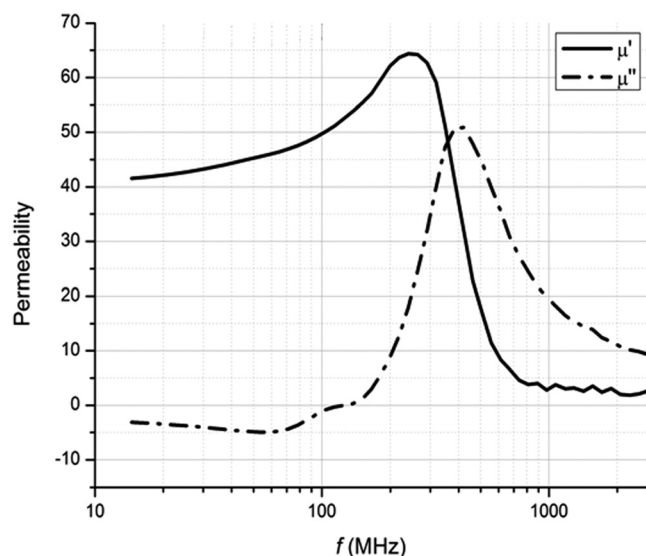


FIG. 1. Complex permeability spectrum of $\text{Ni}_{0.24}\text{Zn}_{0.61}\text{Co}_{0.02}\text{Fe}_{2.13}\text{O}_4$ spin-spray ferrite thin film. Solid line represents real part of permeability μ' and dash line represents imaginary permeability μ'' .

The imaginary permeability has a value of around 20 in the GHz range, and the real permeability is around 42. Some reports indicate that by optimizing the cobalt and zinc content or by changing film thickness, the ferrite film imaginary permeability can reach as high as 100.^{13,14}

B. Crystal structure

Electron microscopy reveals that the films have relatively uniform thickness (~ 250 nm) and flat surfaces. Figure 2(a) shows a low magnification bright-field cross-section TEM image of a sample grown on a glass substrate. The ferrite films have a columnar grain pattern with typical grain widths of ~ 100 nm in diameter. The individual columns are crystalline from the beginning of the chemical deposition reaction. Figure 2(b) is a high-magnification cross-section TEM image showing the morphology of several grains. Growth defects can be seen and coarse Moiré fringes, indicated by "M" are also visible, presumably due to overlapping of two columns in the electron beam direction.

The bright-field TEM image in Fig. 3 shows a ferrite sample deposited on a silicon substrate in plan-view. The ion-milling process was carefully monitored when preparing this sample to ensure removal of the Si substrate while still retaining the ferrite film. Figure 3 clearly reveals the columnar structure of the film with column sizes of 100–200 nm. The differences in diffraction contrast between the columns are caused by different crystal orientations. Brighter areas visible between some grains (marked by white arrows) suggest the possibility of some film porosity, although it is possible that some of these regions are caused by the ion-milling

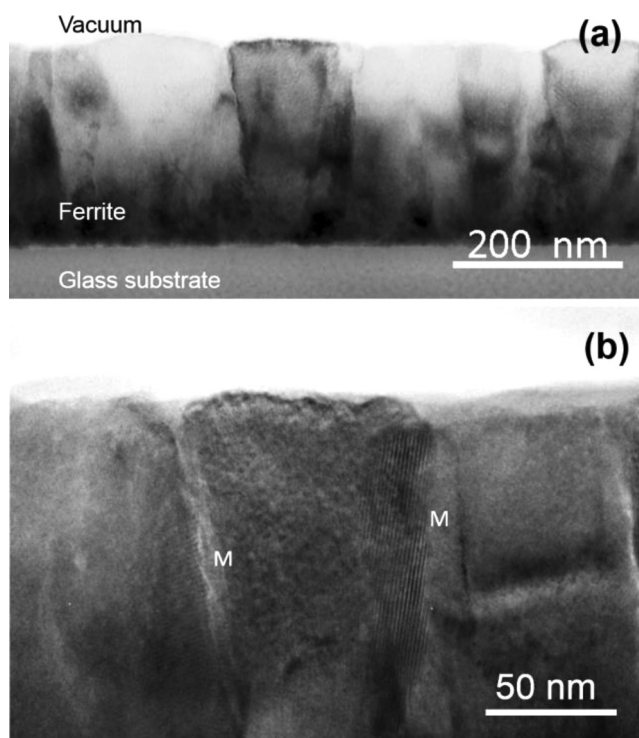


FIG. 2. Low magnification (a), and high-magnification (b), bright-field TEM images showing cross-sections of spin-spray ferrite film deposited on glass substrate.

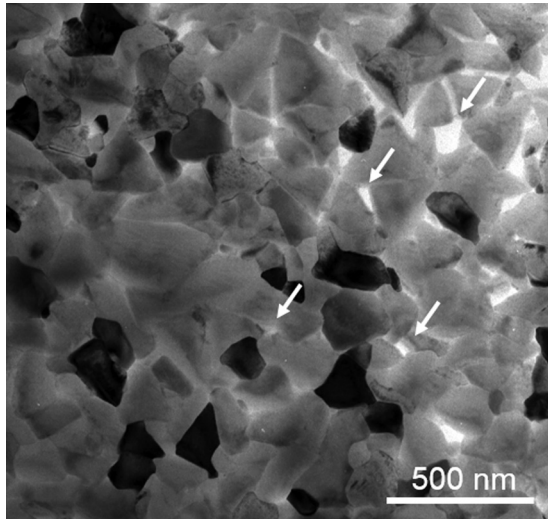


FIG. 3. Plan-view bright-field TEM image showing spin-spray ferrite deposited on silicon substrate. Arrows indicate possible porosity within the film.

process. Some mottling is also visible within single columns (crystal grains) again suggesting the presence of crystal defects such as dislocations and stacking faults.

C. Chemical composition

Annular-dark-field images generated by scanning transmission electron microscope (STEM) are sensitive to atomic number (Z-contrast), and reveal local variations in chemical composition. Figure 4(a) shows a Z-contrast image of the

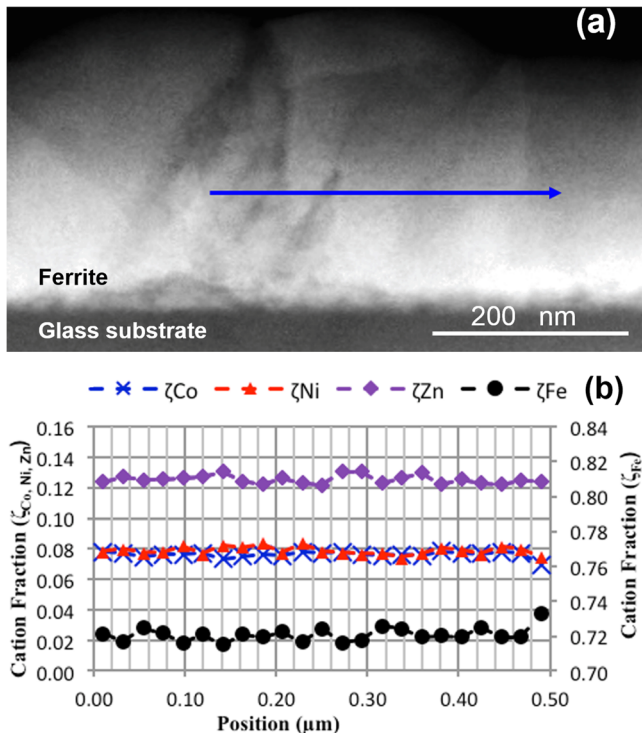


FIG. 4. (a) Cross-section ADF STEM image of spin-spray ferrite film deposited on glass substrate. (b) EDXS line profile from position marked by arrow in (a).

same sample as shown in Fig. 2. The column (grain) boundary regions show darker contrast suggesting that these areas may be amorphous. By using EDXS with a small electron probe, quantitative chemical distribution of different elements can be displayed as a line profile. Figure 4(b) shows EDXS line profiles of nickel, zinc, cobalt, and iron from the line marked by the arrow in Fig. 4(a), converted here into fractional cation values. These compositions are relatively constant across the scanning range, and it can be concluded that there are no compositional inhomogeneities present in the sample at the spatial resolution (~ 2 nm) of this experiment.

D. Magnetic domain structure

Off-axis electron holography is a powerful electron-microscopy technique, which allows the amplitude and phase of the electron wave that has passed through a sample to be determined, rather than its intensity, which is normally the case for imaging.¹⁵ The phase shifts of the electron wave deduced from an electron hologram can then be used to provide quantitative information about the distribution of magnetic fields within and outside the sample with a spatial resolution that can approach the nanometer scale under optimal conditions.¹⁶

In this work, the samples were magnetized *in situ* using the magnetic field of the objective lens of the CM200. With the sample tilted by 30° , the lens current was increased to 1000 mA, providing an in-plane magnetic field of ~ 1 T along the direction of the sample tilt.¹⁶ The objective lens was turned off and the sample was tilted back to horizontal. Holograms were then recorded using the Lorentz mini-lens and CCD camera, with the specimen in a field-free condition.

The magnetic contribution to the phase image in off-axis electron holography can be expressed as¹⁵

$$\varphi(r) = \frac{e}{\hbar} B_{\perp} r t, \quad (1)$$

where φ is the phase, e is the electron charge, \hbar is Planck's constant divided by 2π , r is a direction in the plane of the sample, B_{\perp} is the in-plane magnetic field perpendicular to that direction, and t is the thickness. The gradient of the magnetic phase is then proportional to the perpendicular magnetic field integrated through the thickness of the material

$$\frac{\partial \varphi}{\partial r} = \frac{e}{\hbar} B_{\perp} t. \quad (2)$$

The generated phase map contains not only the magnetic contribution to the phase but also contributions from the sample's mean inner potential,¹⁶ which varies across the field of view and adds difficulty to interpretation of the phase map.¹⁷ To eliminate this effect of the inner potential, one hologram was recorded using the procedure described above. The sample was removed from the microscope and flipped over, and another hologram was then recorded from exactly the same area. Thus, two phase maps are generated, containing the same phase contributions from the mean inner potential but with opposite magnetic contributions. Thus, the mean inner potential contributions to the phase can be removed by subtracting the two images using suitable processing.

Figure 5 shows an example of this procedure applied to a plan-view sample. The area observed was first recorded using the Lorentz lens, as shown in Fig. 5(a). This image has limited magnification but this is still adequate to reveal the columnar structure as well as showing some diffraction contrast. In order to reveal the crystal domain boundary more clearly, the imaging was set to a slightly over-focus condition. The inserted black arrow indicates the direction of the magnetizing field. Figure 5(b) was then obtained from two reconstructed phase images using the subtraction procedure outlined in the paragraph above. The superimposed contour lines correspond to lines of constant phase. No phase information is contained in the noisy areas at the top right and bottom left which were outside the electron interference overlap area in the holograms. Figure 5(c) shows the phase-gradient map obtained from Fig. 5(b), which can be interpreted as a magnetic domain map showing the B_{\perp} distribution. The magnetic field directions are indicated by the colors depicted on the color wheel shown as an inset. Discontinuities due to abrupt diffraction and thickness changes are visible in this gradient map. Based on this gradient map, the positions of magnetic domain walls in the ferrite film can be established, as shown in Fig. 5(d). In order to view the domain structure more clearly, the contrast of the original image has been reversed. The blue arrows indicate the direction of the magnetic induction within each domain.

It is clear from these observations that the size and geometry of the magnetic domains are affected by the crystal morphology. Moreover, single magnetic domains can be formed

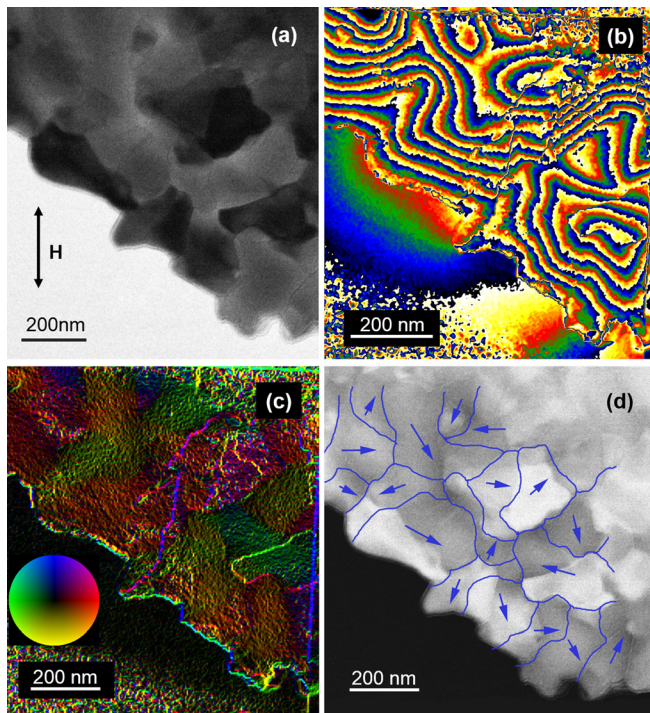


FIG. 5. (a) Image recorded using Lorentz mini-lens. (b) Reconstructed phase map obtained by subtracting two electron holograms to eliminate contribution from mean inner potential. (c) Magnetic domain map. Inserted color wheel indicates the relation between color and magnetic induction direction. (d) Contrast-reversed Lorentz image of (a) with magnetic domains indicated.

by one or several ferrite grains. In some places, the magnetic domain walls follow and coincide with the crystal grain boundaries, while at other places the domain walls cross through individual crystal grains, so that one crystal grain consists of two or more magnetic domains. Although it is hard to rule out the effect of sample shape on domain structure, it seems that most domain walls in the observed area are 90° domain walls [Fig. 5(d)].

It is difficult to construct a model to calculate the sizes of the magnetic domains because the film is not uniform, but the domain sizes can be directly determined. Some grains give strong diffraction contrast in plan-view images which indicates that the orientation is different. However, it is apparent that these grains can also form magnetic domains together with neighboring grains having different crystal orientations. After close examination of high-resolution TEM images of the grain (column) boundary regions, some crystallized areas are found (Fig. 6). Such areas could provide a path for magnetization links between neighboring grains to form single magnetic domains, which would lead to this multiple-grain magnetic domain structure.

In addition to determining the magnetic domain structure of these ferrite films in the remnant state, it is relevant to their potential applications to study domain wall motion or rotation during the magnetization process. Using off-axis holography, it is possible to follow the magnetization status during complete hysteresis loop cycling of magnetic nanostructures.¹⁸ However, phase maps of these ferrite films often include very complicated diffraction contrast features which make it difficult to fully interpret the embedded magnetic information. Here, we only analyze phase gradient maps recorded at remanence after saturation, as shown in Fig. 7. Figure 7(a) shows the phase gradient map of a remnant state. The magnetization process around a complete hysteresis loop was then performed on the sample. The phase gradient map of the new remnant state was recorded in Fig. 7(b). Although the phase contributed by sample thickness is also included in Figs. 7(a) and 7(b) and contributes to the phase gradient, this portion of the phase gradient should be the same in both maps. Thus, the clearly visible differences of the phase gradient

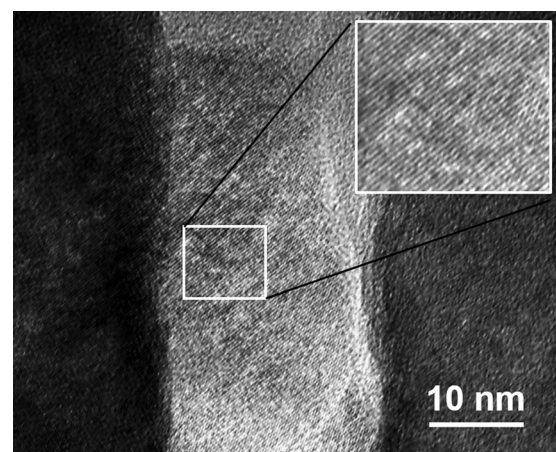


FIG. 6. High-resolution cross-section TEM image of grain boundary region showing presence of crystal lattice fringes.

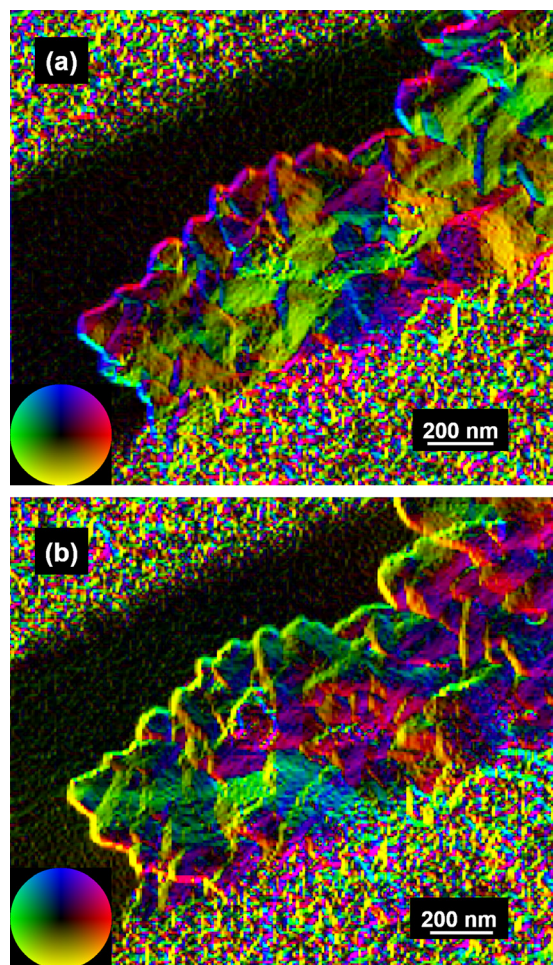


FIG. 7. (a) and (b) Reconstructed phase gradient maps recorded at saturated remnant states before and after magnetization following a complete hysteresis loop.

distribution between these two maps are caused only by the magnetic contribution, indicating that the magnetic domain morphology is not identical for the two remnant states. This result demonstrates that the domain walls did not return to identical positions when the sample was returned to the remnant state. Although it is unclear whether the domain walls rotate or move during our magnetization experiments, the result indicate that there are no preferred magnetization distributions in these ferrite films. Domain wall rotation in this type of ferrite has been observed previously using Lorentz microscopy and under-focus imaging.³ In that work, the applied magnetic field was small (maximum of 130 Oe) and far below saturation. The porosity observed in Fig. 3 which also appears in the ferrite film in Ref. 3 might support the notion of domain-wall pinning.

The holography observations provide information about the in-plane magnetic domain structure of the ferrite films. To check for possible out-of-plane magnetic components, AFM/MFM measurements were also made. However, MFM usually requires a relatively smooth surface, but some residue often attaches to the surface and cannot be removed by regular cleaning. Moreover, SEM imaging (not shown here) also indicated that the surface of the spin-spray ferrite might be too rough for this type of measurement. Cloth polishing

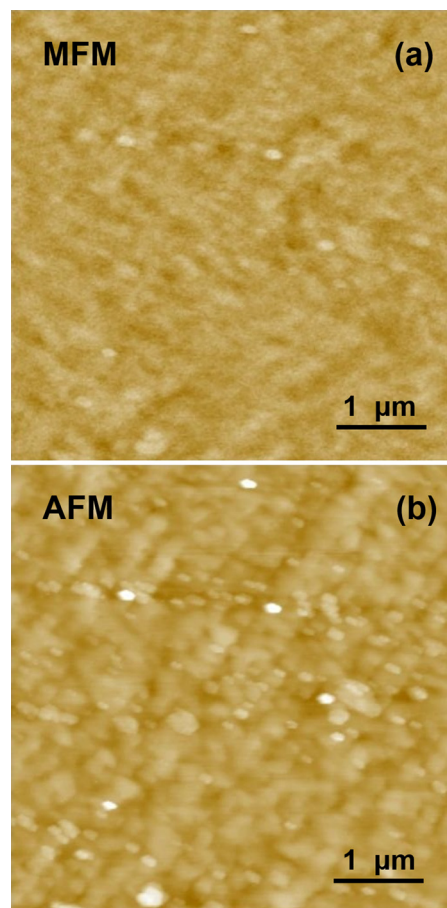


FIG. 8. MFM (a), and AFM (b), images from polished surface of ferrite sample.

plate and artificial diamond solution with average size of 40 nm were thus used to smooth the surface. The AFM and MFM results after polishing are shown in Fig. 8. Some features are visible in the MFM scan [Fig. 8(a)] but these are almost certainly caused by the surface morphology since corresponding features are also visible at the same location in AFM images [Fig. 8(b)]. Moreover, no features resembling magnetic domains are obviously visible in MFM scans. Finally, off-axis electron holography was done on several cross-section samples. The reconstructed phase maps (not shown here) showed no evidence of any magnetic field extending outside the sample. Thus, it can be concluded that the magnetization of the ferrite films must be restricted to in-plane.

IV. CONCLUSIONS

Electron holography and high resolution imaging of the magnetic domain and physical grain structures in nanocrystalline nickel-zinc-cobalt ferrite films reveals that magnetic domains can span across several grains. These observations were conducted on ~ 250 nm-thick films that were grown by aqueous spray deposition onto silicon and glass substrates. Characteristically, the grain microstructures of the films were columnar, comprising of ~ 100 nm diameter grains with their long axes oriented perpendicular to the substrate plane.

Off-axis electron holography of the films in plan-view provided direct evidence that magnetic domains were formed by multiple crystal grains. The magnetic domains were somewhat irregular in shape, with domain walls often following the crystalline grain boundaries, but in some cases crossing through individual grains. Abrupt disruptions in crystal orientation at grain boundaries did not necessarily cause disruption in the orientation of the magnetic domains. Because electron holography is a technique that senses magnetic fields in directions perpendicular to the electron beam, magnetic force microscopic imaging was also carried out on the same material, also in plan-view. The latter results revealed no net magnetic structure perpendicular to the film plane and parallel to the columnar grains, indicating that the internal magnetic fields were oriented in-plane only.

ACKNOWLEDGMENTS

This work was supported by DoE Grant DE-FG02-04ER46168 and material synthesis was funded by Northrup Grumman. We gratefully acknowledge the use of facilities within the John M. Cowley Center for High Resolution Electron Microscopy at Arizona State University, and we acknowledge assistance from the M02 Group, Institute of Physics, Chinese Academy of Science for use of the AFM/MFM facility. The authors thank Sergio Clavijo and Tom Sebastian for their contributions to the permeability measurements.

- ¹A. Goldman, *Modern Ferrite Technology*, 2nd ed. (Springer, Pittsburgh, 2006), p. 273.
- ²N. Ray, "Synthesis and Characterization of Nanocrystalline Nickel-Zinc Spinel Ferrite Thin Films Using the Spin-Spray Deposition Method," Ph.D. dissertation (UMI Proquest, Arizona State University, 2013).
- ³H. Yoshikawa, K. Kondo, S. Yoshida, D. Shindo, and M. Abe, *IEEJ Trans. Electrical Electronic Eng.* **2**, 445–449 (2007).
- ⁴N. Matsushita, C. P. Chong, T. Mizutani, and M. Abe, *J. Appl. Phys.* **91**, 7376 (2002).
- ⁵D. Jiles, *Introduction to Magnetism and Magnetic Materials*, 2nd ed. (Taylor & Francis, New York, 1998).
- ⁶Y. Tamaura, M. Abe, Y. Goto, N. Kitamura, and M. Gomi, *J. Appl. Phys.* **61**, 3211 (1987).
- ⁷N. Matsushita, C. Chong, T. Mizutani, and M. Abe, *IEEE Trans. Magn.* **38**, 3156 (2002).
- ⁸T. Sebastian, S. A. Clavijo, and R. E. Diaz, *J. Appl. Phys.* **113**, 033906 (2013).
- ⁹K. Kondo, S. Yoshida, H. Ono, and M. Abe, *J. Appl. Phys.* **101**, 09M502 (2007).
- ¹⁰K. Kondo, T. Chiba, H. Ono, S. Yoshida, Y. Shimada, N. Matsushita, and M. Abe, *J. Appl. Phys.* **93**, 7130 (2003).
- ¹¹M. Abe, T. Itoh, and Y. Tamaura, *Thin Solid Film.* **216**, 155 (1992).
- ¹²A. K. Subramani, K. Kondo, M. Tada, M. Abe, M. Yoshimura, and N. Matsushita, *Mater. Chem. Phys.* **123**, 16–19 (2010).
- ¹³N. Matsushita, T. Nakamura, and M. Abe, *J. Appl. Phys.* **93**, 7133 (2003).
- ¹⁴N. Matsushita, T. Nakamura, and M. Abe, in *Proceedings of the 2002 IEEE International Magnetism Conference, Amsterdam, Netherland, 28 April–2 May 2002*.
- ¹⁵M. R. McCartney and D. J. Smith, *Annu. Rev. Mater. Res.* **37**, 729 (2007).
- ¹⁶R. E. Dunin-Borkowski, M. R. McCartney, B. Kardynal, S. S. P. Parkin, M. R. Scheinfein, and D. J. Smith, *J. Microsc.* **200**, 187–205 (2000).
- ¹⁷R. E. Dunin-Borkowski, M. R. McCartney, D. J. Smith, and S. S. P. Parkin, *Ultramicroscopy* **74**, 61 (1998).
- ¹⁸H. Hu, H. Wang, M. R. McCartney, and D. J. Smith, *J. Appl. Phys.* **97**, 054305 (2005).